Received March 5, 2020, accepted March 17, 2020, date of publication March 27, 2020, date of current version April 17, 2020.

Digital Object Identifier 10.1109/ACCESS.2020.2983727

Understanding Subsynchronous Oscillation in DFIG-Based Wind Farms With Rotor-Side Converter Control Based on the Equivalent RLC Model

LIN ZHU[1], DANTING ZHONG[1], BEI WANG[2], RONGRUI LIN[1], AND MIN XU[3]

[1]School of Electric Power Engineering, South China University of Technology, Guangzhou 510640, China
[2]State Grid Nantong Electric Power Supply Company, Nantong 226000, China
[3]Electric Power Research Institute of China Southern Power Grid, Guangzhou 510530, China

Corresponding author: Lin Zhu (zhul@scut.edu.cn)

This work was supported by the National Natural Science Foundation of China under Grant U1766213.

ABSTRACT This paper aims to reasonably demonstrate the role of the rotor-side converter (RSC) in subsynchronous oscillation (SSO) and investigates the influence and relationships of all control parameters. Thus, the equivalent circuit of a doubly fed induction generator (DFIG) that considers the RSC is imperative. First, the pertinent equivalent model of a DFIG with RSC control is established. Compared with previous works, this paper innovatively merges the RSC and induction generator with flux and voltage, obtains a complete analytical expression for the equivalent power supply and impedance containing all parameters of both the inner and outer loops of the RSC and then constructs a reasonable equivalent model. The action of the RSC is successfully demonstrated and reflects how the control loops and parameters of the RSC affect the circuit structures and properties of the equivalent model. Then, based on this proposed model, the influence mechanism of the RSC on the SSO of the grid-connected system is carefully analyzed.

INDEX TERMS Doubly fed induction generator, mechanism analysis, rotor-side converter, subsynchronous oscillation.

NOMENCLATURE

RSC	Rotor-side converter.
SSO	Subsynchronous oscillation.
DFIG	Doubly fed induction generator.
VSC-HVDC	Voltage source converter-based high-voltage direct current.
u_s, u_r	Stator and rotor voltage.
i_s, i_r	Stator and rotor current.
ψ_s, ψ_r	Stator and rotor flux linkage.
P_s, Q_s	Stator active and reactive power.
R_s, R_r	Stator and rotor resistance.
L_s, L_r	Stator and rotor inductance.
L_l	Leakage inductance.
L_m	Mutual inductance between the stator and rotor.
p	Differential operator.
s_{slip}	Slip of the rotor to stator currents.
s_{sso}	Slip of the rotor to stator currents at the subsynchronous resonant frequency.
ω_s	Synchronous angular frequency.
ω_{sso}	Subsynchronous angular frequency.
K_{pj}(j=1,2,3,4)	Proportional gains.
K_{ij} (j=1,2,3,4)	Integral gains.
f_0	Synchronous frequency.
f_{sso}	Subsynchronous frequency.
f_{er}	Subsynchronous resonance frequency.
f_r	Rotor frequency.

Subscripts

s, r	Stator and rotor components.
d, q	Direct and quadrature axis components.
ref	Reference value.

The associate editor coordinating the review of this manuscript and approving it for publication was Yang Li.

I. INTRODUCTION

The past few decades have witnessed the rapid growth of wind generation around the world. The DFIG is one of the

most popular wind turbines. DFIGs are usually connected to the grid through a series capacitor-compensated line or a VSC-HVDC link. In such systems, SSO phenomena have recently been frequently reported, for example, in Texas, USA, in 2009 and Hebei, China, in 2012 [1]–[3]. These SSO phenomena have threatened the stability and performance of power systems and are attracting increasing attention to study areas ranging from modeling and mechanism analysis to mitigation actions.

Since these incidents, research communities have devoted significant effort to determining the origin and influencing factors of SSO [4]–[12] by investigating the impacts of converters, the compensation level, and other factors, and the general conclusion is that the RSC is closely related to SSO. For example, [4] shows that the fast and direct properties of the RSC current inner loop are the primary causes of SSO. Reference [5] notes that SSO is susceptible to negative damping at the subsynchronous frequency, and RSC controller parameters have significant impacts on the damping characteristics.

However, the effect of the RSC on SSO, especially considering the RSC controller parameters, is still unclear. In addition, previous studies focused on individual loops or parameters and provided different explanations, and some studies even drew contradictory conclusions. For instance, based on an impedance model, [9] investigates the influence of the RSC controller in series-compensated DFIG-based wind farms on SSO. However, it does not model the outer loop of the RSC controller. Reference [10] explores only the RSC inner control loop and does not consider the impact of its outer control loop. Compared with [9], [10], reference [11] takes the outer control loop into account and suggests not ignoring its influence. However, the authors of [12] do not support this view.

Additionally, the interactive effects of the control loops of the RSC can trigger unfavorable SSO. Recent research shows that parts of the inner and outer control loops of the RSC have an interactive effect on SSO [13], [14]. These papers explain the interactive effects on SSO between the inner-loop proportional gain and the outer-loop proportional gain well. However, they only provide insights into parts of the control loops and controller parameters in the RSC. Undoubtedly, a rigorous research study is required to determine the SSO mechanism caused by the RSC in a DFIG wind farm with series compensation.

Moreover, most researchers adopt various effective methods for investigating SSO, such as the impedance-based method [15], [16], the modal analysis method [17], [18], and the equivalent RLC circuit method [19], [20]; the equivalent RLC circuit method is a simpler and more straightforward approach compared to the other methods. We can easily take all control loops and parameters of the RSC into account when adopting this method. Their roles will be demonstrated using fundamental elements in the equivalent RLC circuit. According to the natural properties of the equivalent circuit, we can analyze and assess the impact of each RSC parameter on SSO and then reveal possible interactive effects under various circumstances.

This paper aims to intuitively identify the influence of the RSC controller on SSO and carry out a thorough and comprehensive review. Considering the RSC, an equivalent RLC model of a series-compensated DFIG-based wind farm is first derived. In this model, the RSC, which acts as a combination of an equivalent source and an RLC circuit, is integrated into the electrical circuit. Thus, the mechanism of how the RSC affects the system dynamics, i.e., SSO, can be thoroughly studied. Not only are the direct and indirect effects of the RSC on SSO both revealed, but the interactive effects between the inner and outer control loops of the RSC on SSO are also entirely identified. Finally, Prony analysis [21] and time-domain simulations verify the proposed model and mechanism.

Compared to existing surveys, this paper provides the following contributions.

a) An improved equivalent RLC model of DFIG is presented. The RSC, including all parameters and control loops, is modeled and derived as an equivalent source with RLC components. We can utilize the relationships between the elements and the natural properties of the equivalent model to intuitively indicate the damping characteristics of the SSO, thereby assessing system stability.
b) How the RSC controller of DFIG affects SSO is fully clarified in this paper. Based on the proposed model, analytical expressions provide insights into the direct and indirect influences. By varying the RSC parameters, the impact of the RSC controller on the equivalent circuit is identified. We can explain why each parameter affects SSO in markedly different ways and efficiently assess their influences.
c) Interactive effects on SSO that involve both the inner and outer loops and even all parameters of the RSC controller are also highlighted. They should be carefully taken into account when optimizing the controller parameters.

The rest of this paper is organized as follows. Section II builds an equivalent DFIG model considering the RSC controller. Section III highlights and explores the mechanism of how the RSC controller influences SSO. In Section IV, Prony analysis and time-domain simulations in PSCAD/EMTDC are performed to verify the proposed model and mechanism. Section V concludes the paper.

II. SYSTEM MODELING

Fig. 1 shows a typical integration of DFIG-based wind farms into a series-compensated transmission system. A single DFIG model representing a DFIG wind farm is built based on the 2-MW generic DFIG model seen in [22].

In this section, we construct a reasonable equivalent model of a DFIG with the RSC controller. Compared with previous works, this paper innovatively merges the RSC and induction

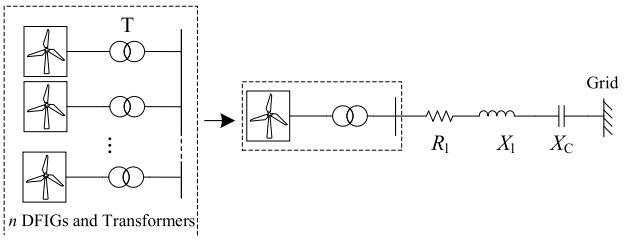

FIGURE 1. Typical wind farm generation model.

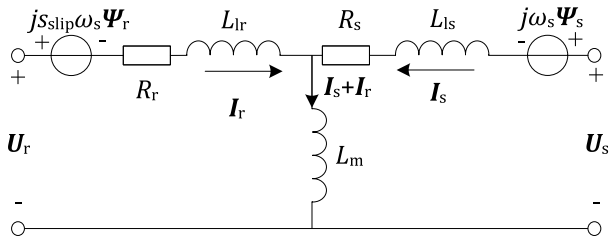

FIGURE 2. Induction generator model.

generator into one circuit using the rotor voltage. According to the Park transformation, transfer functions of the RSC controller and voltage and flux linkage equations of the induction generator can be derived in the rotating d-q reference frame, which act as two individual subsystems: a control subsystem and an electrical subsystem. By moving terms related to the RSC controller and applying the Thevenin theorem, we obtain the rotor voltage equations considering the RSC controller. As an intermediate variable, the rotor voltage bridges these two subsystems. We obtain complete analytical expressions for the equivalent source and impedance containing all parameters of both the inner and outer loops of the RSC. This reasonable equivalent model will play an essential role in the following work.

A. MODELING THE INDUCTION GENERATOR CONSIDERING THE RSC CONTROLLER

The stator and rotor voltage equations and flux linkage equations of the induction generator are given in equations (1)–(4), and Fig. 2 shows the induction generator model.

$$\begin{cases} u_{sd} = R_s i_{sd} + p\psi_{sd} - \omega_s \psi_{sq} \\ u_{sq} = R_s i_{sq} + p\psi_{sq} + \omega_s \psi_{sd} \end{cases} \tag{1}$$

$$\begin{cases} u_{rd} = R_r i_{rd} + p\psi_{rd} - s_{slip}\omega_s \psi_{rq} \\ u_{rq} = R_r i_{rq} + p\psi_{rq} + s_{slip}\omega_s \psi_{rd} \end{cases} \tag{2}$$

$$\begin{cases} \psi_{sd} = L_s i_{sd} + L_m i_{rd} \\ \psi_{sq} = L_s i_{sq} + L_m i_{rq} \end{cases} \tag{3}$$

$$\begin{cases} \psi_{rd} = L_m i_{sd} + L_r i_{rd} \\ \psi_{rq} = L_m i_{sq} + L_r i_{rq} \end{cases} \tag{4}$$

Here, the inductances of the stator and rotor are calculated as L_s=L_{ls}+L_m and L_r=L_{lr}+L_m, respectively.

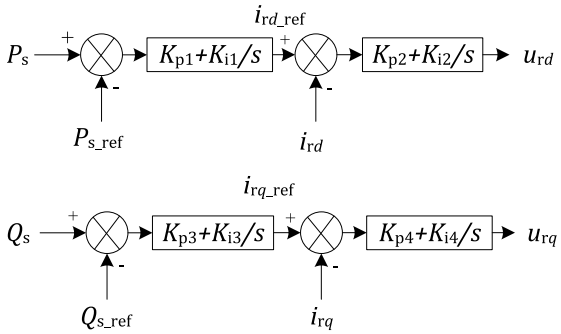

FIGURE 3. RSC controller block diagram.

Based on the RSC controller block diagram shown in Fig. 3, the output voltages of the converter can be expressed as follows.

$$\begin{cases} u_{rd} = \left(K_{p2} + \dfrac{K_{i2}}{s}\right)\left[\left(K_{p1} + \dfrac{K_{i1}}{s}\right)(P_s - P_{sref}) - i_{rd}\right] \\ u_{rq} = \left(K_{p4} + \dfrac{K_{i4}}{s}\right)\left[\left(K_{p3} + \dfrac{K_{i3}}{s}\right)(Q_s - Q_{sref}) - i_{rq}\right] \end{cases} \tag{5}$$

The stator active and reactive powers are

$$\begin{cases} P_s = -\dfrac{U_s L_m}{L_s} i_{rd} \\ Q_s = -\dfrac{U_s^2}{\omega_s L_s} - \dfrac{U_s L_m}{L_s} i_{rq} \end{cases} \tag{6}$$

By substituting (5) into (2), we obtain equation (7), as shown at the bottom of the next page.

To demonstrate the role of the RSC controller, we move terms involving the RSC together and then obtain equation (8), as shown at the bottom of the next page.

From (8), the left-hand sides of the equations consist of two terms. The first terms, -$(K_{p2} + K_{i2}/p)(K_{p1} + K_{i1}/p)P_{sref}$ and -$(K_{p4} + K_{i4}/p)(K_{p3} + K_{i3}/p)Q_{sref}$, are the reference voltages generated by the inner and outer loops for the reference powers, and the second terms can be rewritten as $K_{i1}K_{i2}P_s/\omega^2$ and $K_{i3}K_{i4}Q_s/\omega^2$ in the frequency domain, which are both proportional to $1/\omega^2$. Because ω^2 is high at the synchronous frequency, it can be approximately assumed to be a constant. Thus, the left-hand side of equation (8) can be seen as a controlled voltage source controlled by the converter. Therefore, the rotor voltage considering the RSC controller can be redefined as follows.

$$\begin{cases} u_{rd}^* = -\left(K_{p2} + \dfrac{K_{i2}}{p}\right)\left(K_{p1} + \dfrac{K_{i1}}{p}\right)P_{sref} + \dfrac{K_{i1}K_{i2}}{p^2}P_s \\ u_{rq}^* = -\left(K_{p4} + \dfrac{K_{i4}}{p}\right)\left(K_{p3} + \dfrac{K_{i3}}{p}\right)Q_{sref} + \dfrac{K_{i4}K_{i3}}{p^2}Q_s \end{cases} \tag{9}$$

By substituting (9) into (8), we can obtain equation (10), as shown at the bottom of the next page.

Although equation (10) is intricate, it represents the equivalent resistance, capacitance, and voltage source based on the Thevenin equivalent.

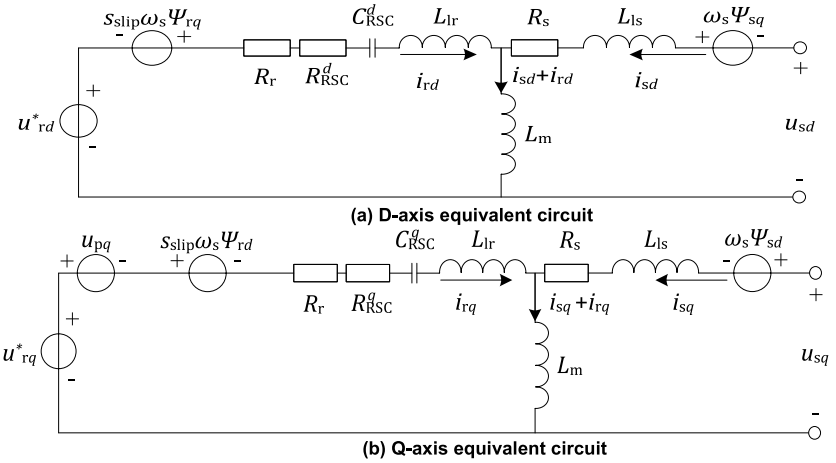

FIGURE 4. Equivalent circuit of the DFIG considering the RSC controller.

Let $R^d_{RSC} = K_{p2}K_{p1}U_sL_m/L_s + K_{p2}$, $R^q_{RSC} = K_{p4}K_{p3}U_s L_m/L_s + K_{p4}$, $1/(C^d_{RSC}p) = K_{i2}/p + (K_{p2}K_{i1}/p + K_{i2}K_{p1}/p) U_sL_m/L_s$, $1/(C^q_{RSC}p) = K_{i4}/p+(K_{p4}K_{i3}/p+K_{i4}K_{p3}/p)U_sL_m/L_s$, $u_{pd} = 0$, and $u_{pq} = (K_{p4}K_{p3}+K_{p4}K_{i3}/p+K_{i4}K_{p3}/p)U_s^2/(\omega_sL_s)$.

Based on equations (1) and (10), an equivalent circuit of a DFIG considering the RSC controller is modeled in the d-q reference frame, as shown in Fig. 4.

B. EQUIVALENT SYSTEM MODEL AT THE SUBSYNCHRONOUS FREQUENCY

By applying stator voltage-oriented control, the RSC can control the active power and reactive power through the d-axis and q-axis rotor currents, respectively. It usually employs proportional-integral controllers in the inner and outer loops. For convenience, we assume that the proportional-integral coefficients of the inner and outer loops in the RSC are identical, meaning that $K_{p1} = K_{p3}$, $K_{i1} = K_{i3}$, $K_{p2} = K_{p4}$, and $K_{i2} = K_{i4}$, as in [23], [24].

On this basis, we combine the d-axis and q-axis components of equation (10) and obtain the following complex vector.

$$U_p = j\left(K_{p4}K_{p3} + \frac{K_{p4}K_{i3}}{p} + \frac{K_{i4}K_{p3}}{p}\right)\frac{U_s^2}{\omega_s L_s} \tag{12}$$

$$\begin{cases} \left(K_{p2} + \dfrac{K_{i2}}{p}\right)\left[\left(K_{p1} + \dfrac{K_{i1}}{p}\right)(P_s - P_{sref}) - i_{rd}\right] = R_r i_{rd} + p\psi_{rd} - s_{slip}\omega_s\psi_{rq} \\ \left(K_{p4} + \dfrac{K_{i4}}{p}\right)\left[\left(K_{p3} + \dfrac{K_{i3}}{p}\right)(Q_s - Q_{sref}) - i_{rq}\right] = R_r i_{rq} + p\psi_{rq} + s_{slip}\omega_s\psi_{rd} \end{cases} \tag{7}$$

$$\begin{cases} -\left(K_{p2} + \dfrac{K_{i2}}{p}\right)\left(K_{p1} + \dfrac{K_{i1}}{p}\right)P_{sref} + \dfrac{K_{i1}K_{i2}}{p^2}P_s \\ = R_r i_{rd} + p\psi_{rd} - s_{slip}\omega_s\psi_{rq} - K_{p2}K_{p1}P_s - \dfrac{K_{p2}K_{i1}}{p}P_s - \dfrac{K_{i2}K_{p1}}{p}P_s + K_{p2}i_{rd} + \dfrac{K_{i2}}{p}i_{rd} \\ -\left(K_{p4} + \dfrac{K_{i4}}{p}\right)\left(K_{p3} + \dfrac{K_{i3}}{p}\right)Q_{sref} + \dfrac{K_{i4}K_{i3}}{p^2}Q_s \\ = R_r i_{rq} + p\psi_{rq} + s_{slip}\omega_s\psi_{rd} - K_{p4}K_{p3}Q_s - \dfrac{K_{p4}K_{i3}}{p}Q_s - \dfrac{K_{i4}K_{p3}}{p}Q_s + K_{p4}i_{rq} + \dfrac{K_{i4}}{p}i_{rq} \end{cases} \tag{8}$$

$$\begin{cases} u^*_{rd} = R_r i_{rd} + \left(K_{p2}K_{p1}\dfrac{U_sL_m}{L_s} + K_{p2}\right)i_{rd} + \left[\dfrac{K_{i2}}{p} + \left(\dfrac{K_{p2}K_{i1}}{p} + \dfrac{K_{i2}K_{p1}}{p}\right)\dfrac{U_sL_m}{L_s}\right]i_{rd} \\ \qquad + L_m p i_{sd} + L_r p i_{rd} - s_{slip}\omega_s\psi_{rq} \\ u^*_{rq} = R_r i_{rq} + \left(K_{p4}K_{p3}\dfrac{U_sL_m}{L_s} + K_{p4}\right)i_{rq} + \left[\dfrac{K_{i4}}{p} + \left(\dfrac{K_{p4}K_{i3}}{p} + \dfrac{K_{i4}K_{p3}}{p}\right)\dfrac{U_sL_m}{L_s}\right]i_{rq} \\ \qquad + L_m p i_{sq} + L_r p i_{rq} + s_{slip}\omega_s\psi_{rd} + \left(K_{p4}K_{p3} + \dfrac{K_{p4}K_{i3}}{p} + \dfrac{K_{i4}K_{p3}}{p}\right)\dfrac{U_s^2}{\omega_s L_s} \end{cases} \tag{10}$$

$$U^*_r = \left(R_r + R_{RSC} + \frac{1}{C_{RSC}p} + L_{lr}p\right)I_r + L_m p\,(I_r + I_s) + js_{slip}\omega_s\psi_r + U_p \tag{11}$$

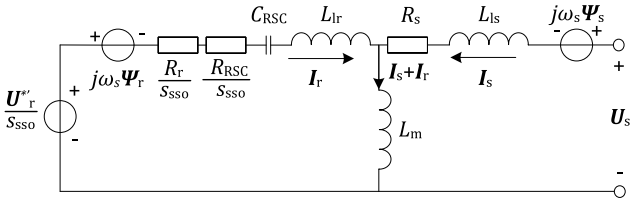

FIGURE 5. Equivalent circuit of the DFIG at the subsynchronous frequency.

At the subsynchronous frequency, the rotor voltage becomes $\boldsymbol{U}_r^*/s_{sso}$, and the equivalent resistance of the DFIG becomes $R_r/s_{sso} + R_{RSC}/s_{sso} + R_s$. In addition, $s_{sso} = (f_{er}\text{-}f_r)/f_{er}$ is the slip of the rotor to the stator current at the subsynchronous resonant frequency $f_{er} = f_0(X_C/\sum X)$, and the subsynchronous frequency is calculated as $f_{sso}=f_0\text{-}f_{er}$. At the subsynchronous frequency, the equivalent circuit of the DFIG is as shown in Fig. 5, where $\boldsymbol{U}_r^{*'} = \boldsymbol{U}_r^* \text{-} \boldsymbol{U}_p$.

Thus, the equivalent resistance and capacitance of the RSC are

$$\frac{R_{RSC}}{s_{sso}} = \frac{K_{p1}K_{p2}\frac{L_m U_s}{L_s} + K_{p2}}{s_{sso}} \tag{13}$$

$$C_{RSC} = \frac{1}{(K_{p2}K_{i1} + K_{p1}K_{i2})\frac{L_m U_s}{L_s} + K_{i2}} \tag{14}$$

C. DISCUSSIONS OF THE MODEL

We provide the following discussions regarding the proposed model.

1) The core idea is to retain both control loops and all parameters of the RSC and then demonstrate their roles in the proposed model. With the intermediate variable of the rotor voltage $\boldsymbol{U}_r$, we successfully fill the gap between the control and electrical subsystems to derive the equivalent circuit. In this circuit, the equivalent source and the frequency-dependent equivalent impedance reflected by the induction generator with the RSC can help in analyzing the mechanism and characteristics of SSO.
2) The equation of the rotor voltage $\boldsymbol{U}_r$ has an additional inner potential term $\boldsymbol{U}_p$. From equation (12), we find that the variations in the controller parameters of the inner and outer loops of the RSC will directly influence the inner potential source and alter the value of the rotor voltage, which reflects the effect of the RSC. However, this voltage cannot change from positive to negative.
3) The frequency-dependent equivalent impedance involves RLC components. Some of it comes directly from the RSC, corresponding to R_{RSC} and C_{RSC}. According to (13), the equivalent resistance R_{RSC} has two terms. The first term is proportional to the product of the inner-loop proportional gain and outer-loop proportional gain $K_{p1}K_{p2}$, and the second term is proportional to the inner-loop proportional gain K_{p2}. According to (14), the equivalent capacitance C_{RSC} is related to all proportional and integral coefficients. Varying the RSC controller parameters will change R_{RSC} and C_{RSC}, which manifests the impact of the RSC controller on the equivalent circuit.

D. THE ADVANTAGES OF THE PROPOSED METHOD OVER EXISTING METHODS

Compared with existing methods, the proposed approach has the following advantages.

a) Unlike modal analysis and impedance-based methods, which require detailed information on each element and significant computational effort, the derived RLC model is simple and easy to establish with little computational effort.
b) The equivalent DFIG model intuitively provides an explicit physical meaning of the oscillation phenomenon based on the equivalent resistance and reactance, thereby directly assessing the system stability and stability margin.
c) Based on the RLC model, the mechanisms of impact of various factors influencing SSO can be clarified, especially the interactive effects between various parameters, while existing methods fail to identify these attributes.

III. THE MECHANISM OF THE IMPACT OF THE RSC ON SSO IN A SERIES-COMPENSATED DFIG-BASED WIND FARM

According to the operating principles of a DFIG, the RSC generates the rotor voltage through the instantaneous power and current and then reacts to the rotor current in the circuit, thereby inducing an additional component in the stator current via magnetic flux. Therefore, when the stator current consists of an oscillating component at the subsynchronous frequency, the instantaneous power of the RSC would be accordingly altered. Next, the converter output voltage, which is disturbed by the RSC controller, causes rotor voltage variation of the DFIG. Then, the rotor voltage affects the rotor current in the circuit and induces an additional subsynchronous component in the stator current. In the above process, the circuit structure and properties have an immense influence on the oscillation component. If the equivalent resistance R_{eq} is >0, then the SSO is positively damped, which means that the SSO will decay. In contrast, if R_{eq} is <0, then negative damping will aggravate the SSO. However, if R_{eq} is ≈ 0, then the SSO amplitude will remain constant. Therefore, the RSC influences the structure and properties of the equivalent DFIG circuit and contributes to determining the oscillation properties.

A. MECHANISM STUDY

The equivalent model of the DFIG considering the RSC controller is connected to the grid through a series-compensated line, as shown in Fig. 6.

As $f_{er} < f_r$, s_{sso} is less than zero at the subsynchronous resonance frequency. In addition, L_m is negligible, given that

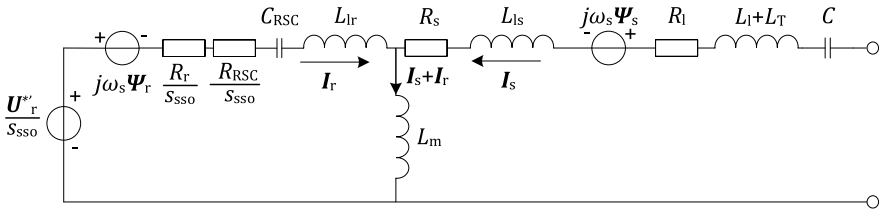

FIGURE 6. Equivalent DFIG circuit of a series-compensated DFIG-based wind farm at the subsynchronous frequency.

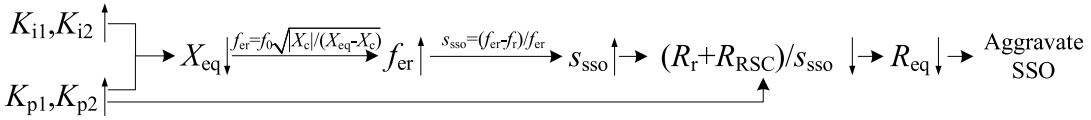

FIGURE 7. Relationship between the RSC and SSO.

L_m is much larger than L_{ls} and L_{lr}. Thus, the equivalent resistance and reactance of the system at the subsynchronous frequency can be expressed as follows.

$$R_{eq} = -\frac{R_r + K_{p1}K_{p2}\frac{L_m U_s}{L_s} + K_{p2}}{|s_{sso}|} + R_s + R_l \qquad (15)$$

The equivalent resistance and reactance, whose expressions contain the control-related terms that reflect the influence of the RSC controller on the circuit structure and properties of the system, can represent the RSC. From equation (15), proportional gains K_{p1} and K_{p2} directly affect the equivalent resistance. Tuning the proportional gains in the RSC may enable the positive resistance to become negative, fundamentally changing the circuit structure and properties of the system. Meanwhile, the slip s_{sso}, which is mainly determined by the equivalent reactance, also has a powerful influence on R_{eq}. According to (16), the equivalent reactance X_{eq} is sensitive to the RSC controller parameters. Modifying the controller parameters can reduce the equivalent reactance X_{eq} of the system, thereby increasing the resonant frequency f_{er} and, finally, increasing the corresponding slip s_{sso}. However, an increase in s_{sso} will reduce the equivalent resistance, thereby aggravating the SSO, and vice versa. The above analysis illustrates the close link between the RSC and SSO in the series-compensated DFIG-based wind farm, as shown in Fig. 7.

According to Fig. 6, when the grid is connected to a line capacitor, the line capacitor and the inductive system form a series resonant circuit. Without a series capacitor, since there is no resonant circuit, SSO is unlikely to occur. That is, the line capacitor plays an important role in SSO. Based on Fig. 7, reducing the line capacitor C, i.e., reducing the capacitive reactance X_C, will increase the resonance frequency f_{er} and its corresponding slip s_{sso} and further reduce the equivalent resistance R_{eq}, aggravating oscillation. Similarly, changing the wind speed can alter the rotor speed, thereby affecting the corresponding slip and the equivalent resistance successively. The above discussion coincides with the conclusions in [5], [20]. Due to space limitations, this paper will not further explore the impact of the line capacitor and wind speed on SSO.

In summary, the RSC has an enormous impact on SSO, which is in accordance with existing research [15]. Furthermore, this paper provides the following new insights into the mechanism and characteristics of the studied impact.

1) Both the direct and indirect mechanisms of how the RSC controller affects SSO are revealed.

The critical point is that the equivalent source and impedance reflected by the RSC controller can be used to identify SSO properties. According to equation (15), the term involving proportional gains shows the direct impact of the RSC on the SSO. In other words, increasing the outer-loop proportional gain K_{p1} and the inner-loop proportional gain K_{p2} can directly reduce the equivalent resistance. Thus, the resistance may change from positive to negative, gradually diminishing the damping of the SSO. From equation (16), the control-related term in the equivalent reactance exerts an indirect effect of the RSC on the SSO. That is, increasing any of the inner-loop and outer-loop proportional and integral coefficients will reduce the equivalent reactance X_{eq} and further increase the resonant frequency f_{er} and the corresponding slip s_{sso}. As a result, the equivalent resistance indirectly decreases. This indirect impact can also change the properties of the equivalent resistance and finally threaten the stability of SSO. The above analysis explicitly explains why the effects of various controller parameters on SSO are markedly different.

$$\begin{aligned} X_{eq} &= X_{lr} + X_{ls} + X_l + X_T + X_{RSC} + X_C \\ &= \omega_{SSO}(L_{lr} + L_{ls} + L_l + L_T) \\ &\quad - \frac{(K_{p2}K_{i1} + K_{p1}K_{i2})\frac{L_m U_s}{L_s} + K_{i2}}{\omega_{SSO}} - \frac{1}{\omega_{SSO}C} \end{aligned} \qquad (16)$$

2) The interactive effects on SSO, which involve both the inner and outer loops and all parameters of the RSC controller, are highlighted.

According to equation (15), the expression of the equivalent resistance contains both an independent term K_{p2} and a coupling term $K_{p1}K_{p2}$. The coupling term indicates that we cannot solely examine the effect of a single parameter on the SSO. Thus, the interactive effect between K_{p1} and K_{p2} should be seriously considered when tuning the controller parameters. Furthermore, coupling terms also exist for the proportional and integral coefficients between the inner and outer loops in the equivalent reactance. The coupling terms $K_{p2}K_{i1}$ and $K_{p1}K_{i2}$ contain all parameters of the RSC controller, denoting the interactive effect between the proportional and integral coefficients in the different control loops on the SSO. A comprehensive investigation of the impact of controller parameters and an exploration of the interactive effects of inner-loop and outer-loop controller parameters on SSO are urgently needed.

B. ANALYSIS AND ASSESSMENT OF INFLUENCING FACTORS

According to (15) and (16), the trends of the effects of all the RSC controller parameters on the equivalent resistance R_{eq} are identical. That is, when the compensation level remains constant, increasing the controller parameters may change the positive resistance to a negative resistance, thereby impairing the oscillation stability.

Under the distinct modes of action of the controller parameters, the controller parameters have notably different levels of influence on the equivalent resistance. While adjusting the proportional gains K_{p1} and K_{p2} can directly change the equivalent resistance, i.e., the equivalent resistance is sensitive to the proportional gains. Conversely, the integral coefficients can only indirectly affect the equivalent resistance through a slight variation in the slip s_{sso}. Thus, the integral coefficients have insignificant effects on the equivalent resistance. We can conclude that the proportional gains influence the SSO more than do the integral coefficients in the same RSC controller.

For the equivalent resistance, the coupling term $K_{p1}K_{p2}$ reflects the constraint between the outer-loop proportional gain and the inner-loop proportional gain. The impact of the single factor K_{p1} on the equivalent resistance will vary with K_{p2}. When tuning K_{p1} within a specific range, increasing K_{p2} will enlarge the equivalent resistance variation, and vice versa. Moreover, the equivalent resistance includes an individual term K_{p2}, which weakens the interactive effect between K_{p1} and K_{p2}. That is, K_{p2} has a considerable impact on the equivalent resistance, even for a small value of K_{p1}. In general, the inner-loop proportional gain K_{p2} of the RSC contributes more to the SSO than does the outer-loop proportional gain K_{p1}.

For the equivalent reactance, we can provide a similar discussion involving all the RSC controller parameters. The coupling terms $K_{p2}K_{i1}$ and $K_{p1}K_{i2}$ demonstrate the constraint between the inner-loop proportional gain K_{p2} (inner-loop integral coefficient K_{i2}) and outer-loop integral coefficient K_{i1} (outer-loop proportional gain K_{p1}). The larger the value of K_{p2} (K_{p1}), the higher the impact of K_{i1} (K_{i2}) on the equivalent reactance. The independent term K_{i2} of the equivalent reactance reduces the restriction between K_{p1} and K_{i2}. The above analysis indicates that K_{i2} has a higher impact on the equivalent reactance than does K_{i1} when $K_{i1}K_{p2}L_mU_s/L_s < K_{i2}K_{p1}L_mU_s/L_s + K_{i2}$.

In conclusion, compared with the outer loop, the inner loop in the RSC exerts a tremendous influence on the SSO. According to the levels of influence on the SSO, we sort all inner and outer controller parameters of the RSC as follows: $K_{p2} > K_{p1} > K_{i2} > K_{i1}$. In the next section, we will verify our studies by Prony analysis and time-domain simulations in PSCAD/EMTDC.

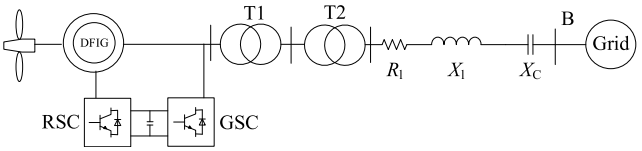

FIGURE 8. A grid-connected DFIG-based wind energy system.

TABLE 1. Controller parameters corresponding to different equivalent resistances.

NUMBER	K_{P1}	K_{P2}	K_{I1}	K_{I2}	R_{EQ} (pu)
1	0.5	0.8	10	20	0.035
2	0.5	1.03	10	20	0.002
3	0.5	1.2	10	20	-0.025

IV. CASE STUDIES

In this section, the impact of the RSC controller on SSO is explored by varying the controller parameters to observe the trajectory of the SSO mode. To verify the proposed studies, we adopt a DFIG wind farm that has a total capacity of 100 MW and is connected to a series-compensated system. The wind farm terminal voltage is successively boosted to 500 kV through transformers T1 (0.69/35 kV) and T2 (35/500 kV). The compensation level in the equivalent system, as viewed from the wind farm, is 50%. The single equivalent model for the DFIG-based wind farm is shown in Fig. 8. In Fig. 8, R_l and X_l represent the line resistance and reactance, respectively, and X_C denotes the series capacitive reactance. All parameters are listed in the Appendix. For the following cases, we assume that the wind speed and compensation level remain constant at 11 m/s and 50%, respectively.

A. CASE A

We choose three groups of RSC controller parameters to exhibit various oscillation properties, as shown in Table 1.

According to equation (15), we can obtain the equivalent resistances corresponding to the three groups of parameters, which are R_{eq1} =0.035 pu, R_{eq2} =0.002 pu, and R_{eq3} = −0.025 pu. The time-domain simulation results for the various parameter settings are displayed in Fig. 9.

From the wind farm output power, we can find various SSO phenomena. For an R_{eq1} of 0.035 pu, positive damping

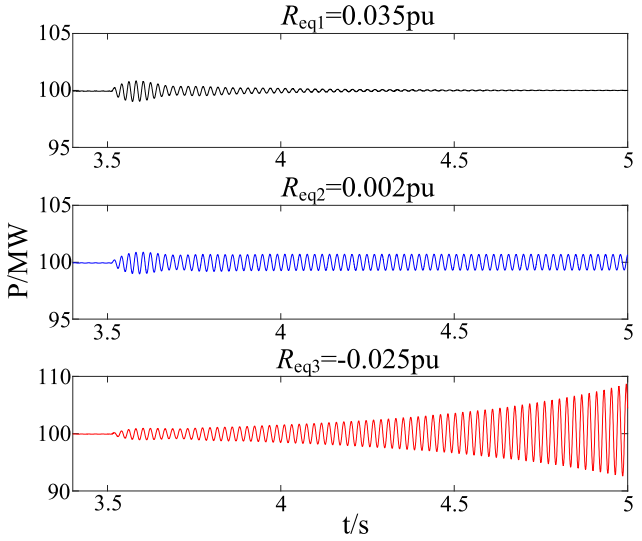

FIGURE 9. Wind farm power curves for different controller parameters.

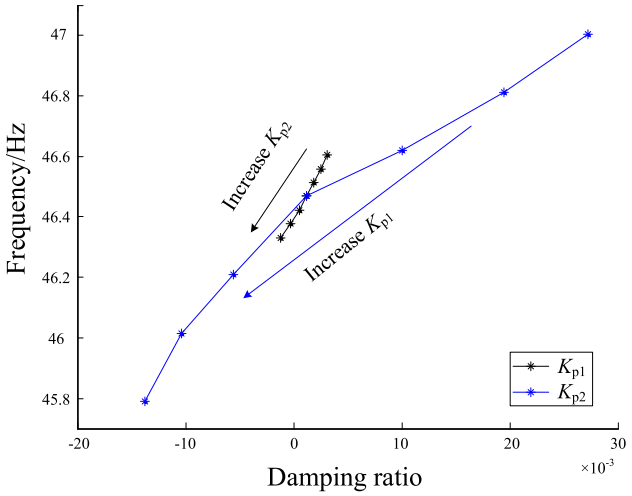

FIGURE 10. Impacts of the proportional gains of the RSC inner and outer loops on the SSO mode.

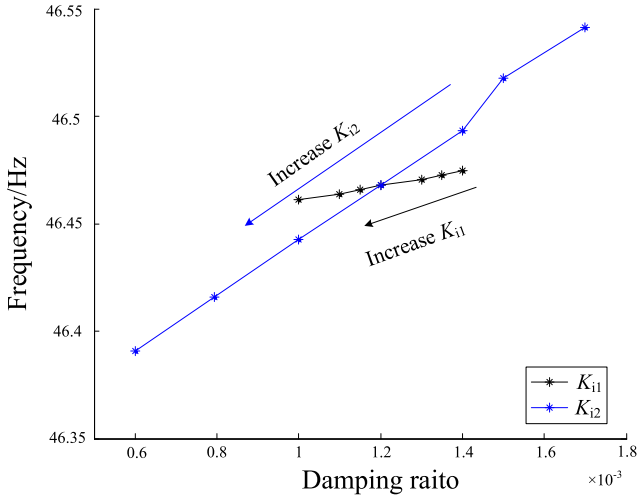

FIGURE 11. Impacts of the integral coefficients of the RSC inner and outer loops on the SSO mode.

is provided for the SSO, such that the active power quickly settles to a steady-state value. For an R_{eq2} approximately equal to zero, the oscillation damping is nearly zero. Thus, the active power oscillates with an almost constant amplitude. For the negative R_{eq3} of -0.025 pu, negative damping is provided for the SSO, such that the active power gradually diverges over time. The simulation results are consistent with the mechanism.

B. CASE B

We set the initial controller parameters as K_{p1} =0.5, K_{p2} =1, K_{i1} =10, and K_{i2} =20. First, the variations in the SSO in the test system are examined when the proportional gains of the rotor-side inner-loop and outer-loop controllers independently vary within the range [−60%, 60%] of their initial values. Prony analysis is applied to the output power data for identification of the oscillation frequency and damping ratio with the above parameter settings, reflecting the effect of parameter variations on the SSO. The trajectories of the SSO mode are shown in Fig. 10.

The results indicate that the trends are similar when we modify the proportional gains in the RSC controller. If we increase the proportional gains of the inner and outer loops, the damping ratio of the SSO mode will be reduced. In some scenarios, the damping ratio can change from positive to negative, resulting in system instability. In addition, within the same range of parameters, oscillation damping is more sensitive to K_{p2} than to K_{p1}.

Similarly, when the inner-loop and outer-loop integral coefficients independently change from −60% to 60% of their initial values, the trajectory of the SSO mode is as presented in Fig. 11. This figure illustrates that the higher the integral coefficients of the RSC controller, the lower the damping of the SSO mode, which is analogous to the effect of the proportional gains. Additionally, within the same range of integral coefficients, K_{i2} has a larger impact on the damping ratio than does K_{i1}. In contrast to the proportional gains, the integral coefficients cannot be modified to change the damping ratio from positive to negative, denoting notably different effects on the SSO.

In summary, when the other parameters, such as the wind speed and compensation level, remain constant, increasing the RSC controller parameters will lower the equivalent resistance, which will reduce oscillation damping and can even lead to the positive damping changing to negative damping. Concerning the RSC control loops, SSO is more sensitive to the inner loop than to the outer loop. Regarding the RSC controller parameters, the proportional gains exert a stronger influence on SSO than do the integral coefficients. The simulation results are consistent with the analyzed mechanism in section III and confirm the given order of the controller parameters, which is $K_{p2} > K_{p1} > K_{i2} > K_{i1}$.

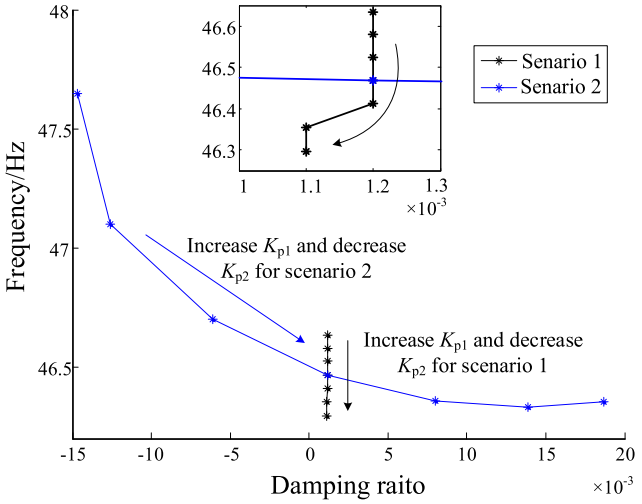

FIGURE 12. Impacts of Kp1 and Kp2 on the SSO mode for Scenario 1 and Scenario 2.

TABLE 2. A comparison between the equivalent resistances and damping ratios of the SSO mode for scenario 1 and scenario 2.

K_{P1}	SCENARIO 1			SCENARIO 2		
	K_{P2}	R_{EQ}(pu)	σ	K_{P2}	R_{EQ}(pu)	σ
0.2	1.245	0.0043	0.0012	2.5	-0.0175	-0.0147
0.3	1.151	0.0041	0.0012	1.667	-0.0084	-0.0126
0.4	1.07	0.0037	0.0012	1.25	-0.0024	-0.0061
0.5	1	0.0034	0.0012	1	0.0034	0.0012
0.6	0.938	0.0032	0.0012	0.833	0.0091	0.008
0.7	0.883	0.003	0.0011	0.714	0.0143	0.0139
0.8	0.835	0.0029	0.0011	0.625	0.019	0.0187

C. CASE C

To demonstrate the interactive effects among the distinct parameters and control loops in the RSC, we design the following three scenarios.

1) SCENARIO 1: KP1 AND KP2 ARE SIMULTANEOUSLY ALTERED, WHILE KP1KP2LMUS/LS+KP2 REMAINS UNCHANGED

The variations in the SSO mode and wind power curves in the DFIG-based wind power system are displayed in Fig. 12 and Fig. 13, respectively. The comparison between the equivalent resistances and damping ratios for Scenario 1 and Scenario 2 are shown in Table 2.

In this case, R_{eq} is affected only by the variation in s_{sso}. Therefore, modifying K_{p1} and K_{p2} can only change X_{eq} to indirectly alter s_{sso}. Due to the slight variation in s_{sso}, R_{eq} is approximated as a constant; thus, the damping variation of the SSO mode is negligible. These simulation results validate the analysis in section III.

2) SCENARIO 2: KP1 AND KP2 ARE SIMULTANEOUSLY ALTERED, WHILE KP1KP2 REMAINS CONSTANT

The trajectory of the SSO mode and the output power of the wind farm in Scenario 2 are shown in Fig. 11 and Fig. 14, respectively.

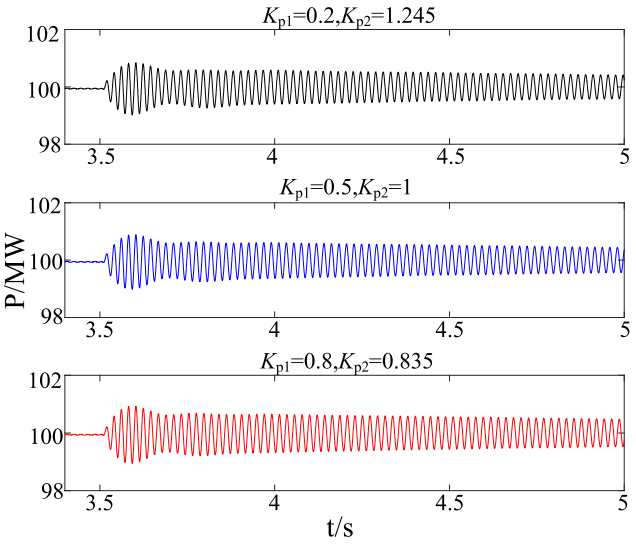

FIGURE 13. Wind farm power curves for Scenario 1.

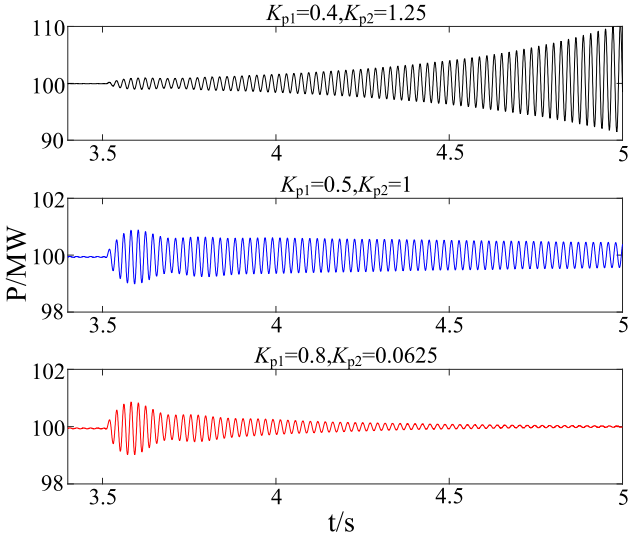

FIGURE 14. Wind farm power curves for Scenario 2.

The results obtained in this scenario demonstrate the interactive effect between K_{p1} and K_{p2}. When the coupling term $K_{p1}K_{p2}$ in R_{eq} remains constant, the higher the value of K_{p1}, the lower the value of K_{p2}. According to equation (15), as the independent term K_{p2} decreases, the equivalent resistance increases, thereby improving the damping ratio of the SSO, which validates the mechanism presented in section III.

3) SCENARIO 3: THREE GROUPS OF KP1 AND KP2 ARE SET, AND THEN, KI1 AND KI2 ARE INDEPENDENTLY TUNED WHILE KP1KP2LMUS/LS+KP2 IS KEPT CONSTANT

This scenario aims to validate the interactive effects among all controller parameters in the RSC. Three sets of K_{p1} and K_{p2} are taken as follows: (1) K_{p1} =1 and K_{p2} =0.8, (2) K_{p1} =1.29 and K_{p2} =0.7, and (3) K_{p1} =1.67 and K_{p2} =0.6. We set the initial values of K_{i1} and K_{i2} as 20 and 40, respectively, and independently tune them within the range

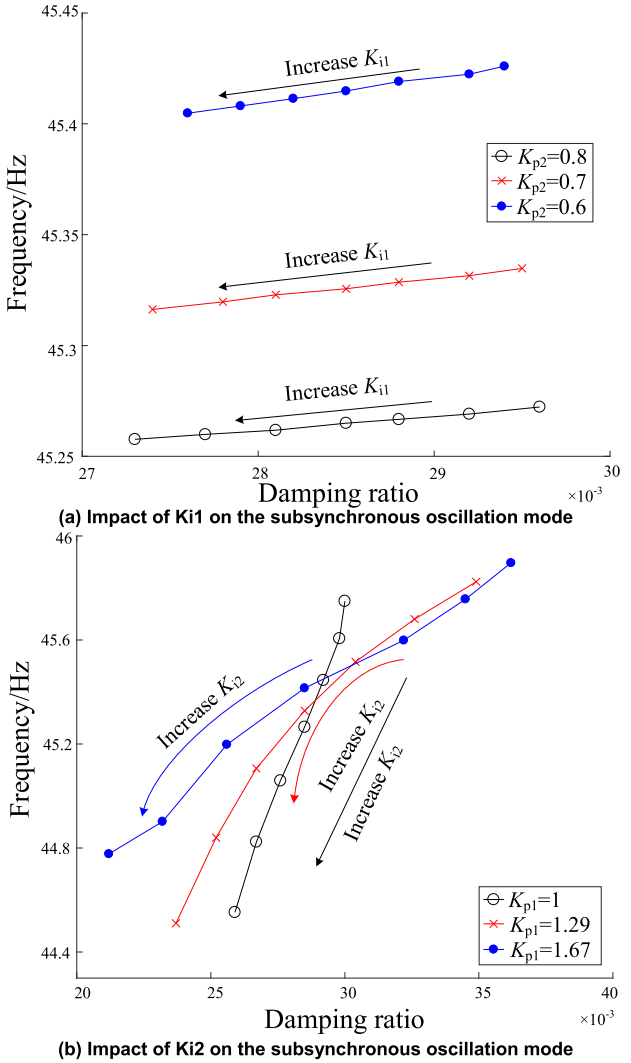

FIGURE 15. Impacts of the integral coefficients of the RSC inner and outer loops on the SSO mode in Scenario 3.

TABLE 3. Parameters of a doubly fed induction generator.

Parameter	Value
nominal power	2MW
nominal frequency	50Hz
nominal voltage	690V
stator resistance	0.0054p.u.
stator leakage inductance	0.1p.u.
rotor resistance	0.00607p.u.
rotor leakage inductance	0.11p.u.
magnetizing inductance	4.5p.u.
DC link rated voltage	1.15kV

TABLE 4. Control parameters of a doubly fed induction generator.

Controller	Parameter	Value	Bandwidth
RSC	outer proportional gain, K_{p1}	0.5	11Hz
	outer integral gain, K_{i1}	10	
	inner proportional gain, K_{p2}	1	185Hz
	inner integral gain, K_{i2}	20	
GSC	outer proportional gain, K_{p3}	0.2	30Hz
	outer integral gain, K_{i3}	10	
	inner proportional gain, K_{p4}	1	240Hz
	inner integral gain, K_{i4}	80	
PLL	proportional gain, K_{p_PLL}	60	80Hz
	integral gain, K_{i_PLL}	1200	

from −60% to 60% of their initial values. The trajectories of the SSO modes are shown in Fig. 15.

In this case, based on the investigated mechanism, all controller parameters can only affect the equivalent reactance and then alter s_{sso} to indirectly modify R_{eq} for the distinct groups of proportional gains. Given the coupling term in equation (16), we ensure that the equivalent reactance is only affected by the parameters to be adjusted. Thus, based on this premise, we set various $K_{p2}(K_{p1})$ but keep $K_{p1}K_{p2}L_mU_s/L_s + K_{p2}$ unchanged, and the impact of K_{i1} (K_{i2}) on the variation in the SSO mode can be examined.

The simulation results demonstrate that, with a constant $K_{p2}(K_{p1})$, an increase in $K_{i1}(K_{i2})$ will lower the damping ratio of the SSO mode, and K_{i2} has an enormous impact on the SSO compared to K_{i1}. The discrepancy arises from the levels of influence of K_{i1} and K_{i2} on the SSO. The higher the value of K_{p2}, the more susceptible the damping ratio is to K_{i1}. Likewise, upon increasing K_{p1}, the results for K_{i2} are similar to those described above. The above discussion intuitively explains the interactive effect between $K_{p2}(K_{p1})$ and $K_{i1}(K_{i2})$, as well as the influence of the individual term K_{i2}.

As the proportional coefficients have both direct and indirect impacts on the SSO, it is hard to investigate how the integral coefficients affect the interactive effect of the gain coefficients. However, scenario 3 can help to validate the interactive effects among all controller parameters in the RSC.

V. CONCLUSION

This paper establishes an improved RLC model, which includes all parameters and control loops of the RSC, to assess and investigate the mechanism of the RSC controller on SSO. Based on the model, the role of the RSC in SSO can be represented as a combination of an equivalent source and an equivalent impedance. Then, we can conclude that variations in the RSC controller parameters have large impacts

TABLE 5. Parameters of the transformer and line.

Parameter	Value
line resistance, R_l	0.02 p.u.
line reactance, X_l	0.50 p.u.
transformer reactance, X_T	0.14 p.u.

on the structures and properties of the equivalent circuit, affecting the properties of the SSO. The studied mechanism provides an explicit explanation of the RSC controller effect on SSO and can be further extended to assess the factors of SSO.

Additionally, this paper provides new insights. The RSC can directly and indirectly affect the SSO through the equivalent resistance and reactance, respectively. In addition, the expression of the equivalent reactance reveals the interactive effects between the inner and outer control loops and all the parameters of the RSC controller on SSO. These interactive effects should be carefully considered when designing a controller. Finally, three cases are designed to validate the proposed studies.

APPENDIX

See Table 3–5.

REFERENCES

[1] J. Adams, C. Carter, and S.-H. Huang, "ERCOT experience with subsynchronous control interaction and proposed remediation," in *Proc. PES*, Orlando, FL, USA, May 2012, pp. 1–5.

[2] D. Kidd and P. Hassink, "Transmission operator perspective of subsynchronous interaction," in *Proc. PES*, Orlando, FL, USA, May 2012, pp. 1–3.

[3] F. Zhao, L. Wu, J. Zhang, X. Gao, H. Liu, H. Wang, and Y. Yang, "Suppression method of parallel-damping controller for DFIG," *J. Eng.*, vol. 2017, no. 13, pp. 880–884, Jan. 2017.

[4] G. D. Irwin, A. K. Jindal, and A. L. Isaacs, "Sub-synchronous control interactions between type 3 wind turbines and series compensated AC transmission systems," in *Proc. IEEE Power Energy Soc. Gen. Meeting*, Detroit, MI, USA, Jul. 2011, pp. 1–6.

[5] L. Wang, X. Xie, Q. Jiang, H. Liu, Y. Li, and H. Liu, "Investigation of SSR in practical DFIG-based wind farms connected to a series-compensated power system," *IEEE Trans. Power Syst.*, vol. 30, no. 5, pp. 2772–2779, Sep. 2015.

[6] Y. Xu and S. Zhao, "Mitigation of subsynchronous resonance in series-compensated DFIG wind farm using active disturbance rejection control," *IEEE Access*, vol. 7, pp. 68812–68822, 2019.

[7] C. Gao, H. Liu, H. Jiang, Y. Li, and X. Tang, "Research on the subsynchronous oscillation in wind power connected to series compensated power system and its influencing factors," *CES Trans. Electr. Mach. Syst.*, vol. 3, no. 1, pp. 334–340, Sep. 2017.

[8] J.-L. Su, L.-B. Shi, L.-Z. Yao, Y.-X. Ni, S.-Y. Qin, R.-M. Wang, and J.-P. Zhang, "Sub-synchronous resonance analysis of grid-connected DFIG- based wind farms," in *Proc. Int. Conf. Power Syst. Technol.*, Chengdu, China, Oct. 2014, pp. 2812–2818.

[9] Z. Miao, "Impedance-model-based SSR analysis for type 3 wind generator and series-compensated network," *IEEE Trans. Energy Convers.*, vol. 27, no. 4, pp. 984–991, Dec. 2012.

[10] A. Ostadi, A. Yazdani, and R. K. Varma, "Modeling and stability analysis of a DFIG-based wind-power generator interfaced with a series-compensated line," *IEEE Trans. Power Del.*, vol. 24, no. 3, pp. 1504–1514, Jul. 2009.

[11] P.-H. Huang, M. S. El Moursi, W. Xiao, and J. L. Kirtley, "Subsynchronous resonance mitigation for series-compensated DFIG-based wind farm by using Two-Degree-of-Freedom control strategy," *IEEE Trans. Power Syst.*, vol. 30, no. 3, pp. 1442–1454, May 2015.

[12] K. Sun, W. Yao, J. Fang, X. Ai, J. Wen, and S. Cheng, "Impedance modeling and stability analysis of grid-connected DFIG-based wind farm with a VSC-HVDC," *IEEE J. Emerg. Sel. Topics Power Electron.*, early access, Feb. 28, 2019, doi: 10.1109/jestpe.2019.2901747.

[13] X. Wu, Y. Guan, W. Ning, P. Jiang, and Y. Xu, "Mechanism of Interactive Effect of RSC Parameters in DFIG on SSO and its Application," (in Chinese), *Power Syst. Technol.*, vol. 42, no. 08, pp. 2536–2544, Aug. 2018.

[14] W. Ning, X. Wu, Y. J. Guan, and F. Chen, "Method to suppress sub-synchronous oscillation of DFIG-based wind farms based on virtual impedance," *J. Eng.*, vol. 2017, no. 13, pp. 2173–2177, Jan. 2017.

[15] L. Fan and Z. Miao, "Nyquist-stability-criterion-based SSR explanation for Type-3 wind generators," *IEEE Trans. Energy Convers.*, vol. 27, no. 3, pp. 807–809, Sep. 2012.

[16] X. Zhang, X. Xie, H. Liu, and Y. Li, "Robust subsynchronous damping control to stabilise SSR in series-compensated wind power systems," *IET Gener., Transmiss. Distrib.*, vol. 13, no. 3, pp. 337–344, Feb. 2019.

[17] K. Gu, F. Wu, X.-P. Zhang, P. Ju, H. Zhou, J. Luo, and J. Li, "SSR analysis of DFIG-based wind farm with VSM control strategy," *IEEE Access*, vol. 7, pp. 118702–118711, 2019.

[18] R. K. Varma and A. Moharana, "SSR in double-cage induction generator-based wind farm connected to series-compensated transmission line," *IEEE Trans. Power Syst.*, vol. 28, no. 3, pp. 2573–2583, Aug. 2013.

[19] X. Xie, X. Zhang, H. Liu, H. Liu, Y. Li, and C. Zhang, "Characteristic analysis of subsynchronous resonance in practical wind farms connected to series-compensated transmissions," *IEEE Trans. Energy Convers.*, vol. 32, no. 3, pp. 1117–1126, Sep. 2017.

[20] H. Liu, X. Xie, C. Zhang, Y. Li, H. Liu, and Y. Hu, "Quantitative SSR analysis of series-compensated DFIG-based wind farms using aggregated RLC circuit model," *IEEE Trans. Power Syst.*, vol. 32, no. 1, pp. 474–483, Jan. 2017.

[21] D. Potts and M. Tasche, "Parameter estimation for nonincreasing exponential sums by prony-like methods," *Linear Algebra Appl.*, vol. 439, no. 4, pp. 1024–1039, Aug. 2013.

[22] M. Edrah, K. L. Lo, and O. Anaya-Lara, "Reactive power control of DFIG wind turbines for power oscillation damping under a wide range of operating conditions," *IET Gener., Transmiss. Distrib.*, vol. 10, no. 15, pp. 3777–3785, Nov. 2016.

[23] H.-S. Ko, G.-G. Yoon, and W.-P. Hong, "Active use of DFIG-based variable-speed wind-turbine for voltage regulation at a remote location," *IEEE Trans. Power Syst.*, vol. 22, no. 4, pp. 1916–1925, Nov. 2007.

[24] L. Xu and Y. Wang, "Dynamic modeling and control of DFIG-based wind turbines under unbalanced network conditions," *IEEE Trans. Power Syst.*, vol. 22, no. 1, pp. 314–323, Feb. 2007.

LIN ZHU received the Ph.D. degree from the South China University of Technology (SCUT), Guangzhou, China, in 2007. He has been an Associate Professor with the School of Electrical Power Engineering, SCUT, since 2007. His research interests include HVDC, power system modeling, and stability and control.

DANTING ZHONG received the B.S. degree in electrical engineering from the South China University of Technology (SCUT), Guangzhou, China, in 2018, where she is currently pursuing the M.S. degree in power systems and automation. Her research interests include HVDC, wind farms, and power system stability and control.

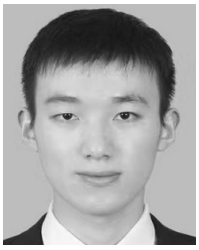

BEI WANG received the M.S. degree from the South China University of Technology (SCUT), Guangzhou, China, in 2019. His research interests include HVDC, power system stability, and control and wind power.

RONGRUI LIN is currently pursuing the bachelor's degree with the School of Electrical Power Engineering, South China University of Technology (SCUT). His research interests include power system stability and system modeling.

MIN XU received the Ph.D. degree from the South China University of Technology (SCUT), Guangzhou, China, in 2014. He is currently a Senior Engineer with the Electric Power Research Institute of China Southern Power Grid. His research interests include power system stability and control, HVDC, and distribution networks.